Finite Element Simulation of Friction Stir Welding of Inconel 718 to Nimonic 80A

Tom Saju and M. Velu*

School of Mechanical Engineering, Vellore Institute of Technology, Vellore, Tamil Nadu, India
E-mail: tom.saju2019@vitstudent.ac.in; mvelu@vit.ac.in
**Corresponding Author*

Received 13 February 2021; Accepted 16 March 2021;
Publication 06 May 2021

Abstract

This paper presents results of simulation of friction stir dissimilar welding of 5 mm thick, Nickel-based super-alloys, Inconel 718, and Nimonic 80A using Abaqus software. Four different trials were done to understand the influence of tool rotation speed on temperature distribution in weld zone while travel speed remains constant. The temperature in the weld zone was found to increase with the increase in tool rotation speed and travel speed. The temperature on the advancing side of the tool was higher than that of the retreating side. The tensile strength of weldment was found, by simulation, to be 25% more than that of base metal, Inconel 718. This may be due to grain refinement and dynamic recrystallization during FSW. The simulated bend test revealed an adequate level of ductility of weldments.

Keywords: Friction stir welding, Nickel-based super-alloy, Abaqus software, grain refinement, dynamic recrystallization.

1 Introduction

Friction Stir Welding (FSW) finds application in industries such as aerospace, shipbuilding, automobile, railways, and robotics [1]. The fig-tree arrangement

European Journal of Computational Mechanics, Vol. 29_4–6, 417–436.
doi: 10.13052/ejcm1779-7179.29465

used in turbine blades and discs of aerospace industries is subjected to failure while in service. Hence, welding techniques are preferred in recent times as an alternative for mechanical joints [2]. Multi-metal components, in particular, the dissimilar ones prefer solid-state welding techniques like FSW, as fusion welding causes the formation of intermetallic compounds, embrittlement, porosity, cracking, segregation, grain growth, etc. which are detrimental to the strength of the weldments [3].

FSW provides high-quality joints with more energy efficiency for both similar and dissimilar materials. Heat generation due to friction between the rotating tool and workpiece material causes plastic deformation that helps in the joining of materials. No flux, gas, or filler material is necessary for FSW. A rotating tool plunges into the edges of the base material and a transverse movement along the welding edges causes welding. Both forging and extrusion processes are together applied in the FSW process. The movement of the tool pin creates localized heating that contributes to softening of the material. Both translation and tool rotation creates movement of the material from the front of the tool pin towards the back of the pin. Plastic deformation due to frictional heating results in the formation of equiaxed and fine recrystallized grains that results in good mechanical properties [4]. FSW has two sides, the advancing side and the retreating side based on the direction of tool movement. For the advancing side, both the tool direction and velocity vectors of the rotating tool are the same. While for the retreating side, tool direction and velocity vectors are in opposite directions. During FSW, temperature due to friction rises to 80–90% of the melting point of the base material [5].

Tool for friction stir welding was selected based on two important considerations namely weld quality and tool wear [6]. Intense stirring and mixing of the material is the result of an increase in tool rotation rate and tool movement in transverse direction respectively [7]. Sound welds are produced by controlling the insertion depth of the pin into the shoulders [8, 9]. Tool stresses during initial plunging can be reduced using preheating technique [10]. Figure 1 shows the schematic diagram for the friction stir welding technique.

Numerical simulation technique is widely used in industries that help to predict any defects within weld that can cause a serious failure. P Giles in his paper on numerical simulation of welding explained a simulation model for welding incorporating 3D analysis in welding. In his paper, he simulated TIG welding using SYSWELD software [11]. Thomas Dupuy developed a numerical simulation model for resistance welding through

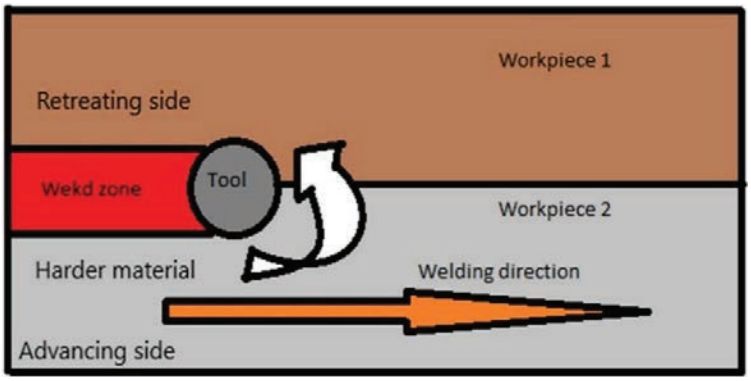

Figure 1 Schematic diagram for friction stir welding.

electro-thermal coupling [12]. R Fortunier developed a thermo-mechanical model to understand distortion happening during welding [13].

The main objective of this paper is to simulate and predict various characteristics of the FSW process using a commercially available Abaqus finite element package. Two dissimilar Ni-based super-alloys, generally used in gas turbine discs and blades namely Inconel 718 and Nimonic 80A were chosen as the base metals for welding. The influence of tool rotation speed and travel speed on temperature distribution was studied. Also, the tensile strength and ductility of the weldments were predicted using Abaqus simulation.

2 Model Description

FSW simulation is a complex procedure as it involves both mechanical and thermal phenomena. The base metals of this study, Inconel 718 and Nimonic 80A are nickel-based super-alloys known for their excellent high-temperature properties and ability to withstand extreme operating environments. Table 1 shows the chemical compositions of both the alloys. The base metals were modeled as plates of dimension 150 mm $\times$ 60 mm $\times$ 5 mm each. Tungsten carbide (WC-Co) tool with shoulder diameter of 20 mm, pin diameter of 7 mm and tool pin length of 4.8 mm was selected for this study. Figure 2 explains the model dimensions of base metals and the FSW tool.

The transverse cross-section of the weld was selected for tensile testing with the weld zone towards the center of the specimen. Dimensions of tensile test specimen as shown in Figure 3 were conforming to ASTM E8-M16. The

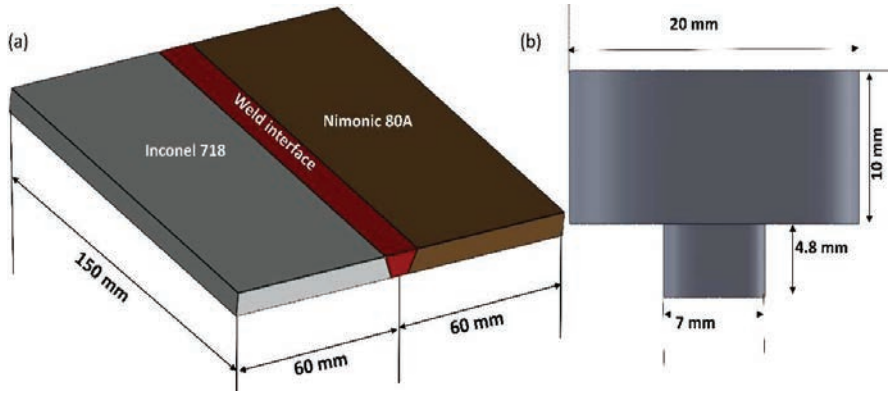

Figure 2 Schematic diagram of (a) butt joint configuration for FSW and (b) FSW tool.

Table 1 Chemical composition of Inconel 718 and Nimonic 80A [14, 15]

	Ni	Cr	Fe	Mo	Nb	Co	Mn	Al	Ti	Si	C
Inconel 718	50–55	17–21	11.2–22.5	2.8–3.3	4.7–5.5	1.0	0.3	0.6–1.1	0.3	0.3	0.08
Nimonic 80A	Balance	18–21	3.0 max	–	–	2.0	1.0	1–1.8	1.8–2.7	1.0	0.10

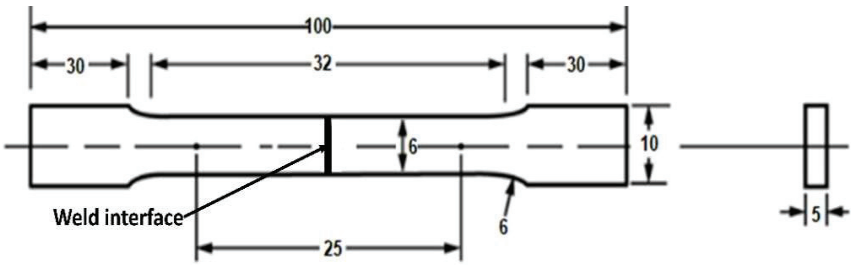

Figure 3 Schematic diagram of transverse (weld joint) tensile test specimen.

gauge length of 25 mm, the thickness of 5 mm, and a total length of 100 mm were chosen.

Table 2 shows the welding parameters selected for different trials. Tool rotation speed and weld travel speed were varied to understand its influence on temperature distribution while tool downward force was constant at 39.2 kN. Tool rotation speed was increased from 400 rpm to 1300 rpm in steps of 100 rpm with tool travel speed kept constant for the first three trails, namely R1, R2, and R3. In trail R4, tool rotation speed was maintained

Table 2 Welding parameters of FSW

Trials	Tool Rotation Speed (rpm)	Tool Travel Speed (Welding Speed) (mm/min)	Tool Downward Force (N)
R1	400, 500, 600, 700, 800, 900, 1000, 1100, 1200, 1300	40	39.2×10^3
R2	400, 500, 600, 700, 800, 900, 1000, 1100, 1200, 1300	60	39.2×10^3
R3	400, 500, 600, 700, 800, 900, 1000, 1100, 1200, 1300	80	39.2×10^3
R4	1300	40, 50, 60, 70, 80, 90, 100	39.2 x 10^3

Table 3 Material constants of Johnson-Cook relation [17, 18]

	A	*B*	*C*	*n*	*m*	Melting Point (°C)
Inconel 718	1108	699	0.0085	0.5189	1.2861	1593
Nimonic 80A	487	2511	0.0116	0.983	1.162	1365

constant at 1300 rpm while tool travel speed was increased from 40 mm/min to 100 mm/min in equal increments of 10 mm/min. Finally, the influence of tool rotation speed and travel speed on temperature distribution was plotted.

Finite element analysis of friction stir welding using Abaqus/explicit software is achieved using coupled Eulerian-Lagrangian formulation, Coulomb's law of friction, and the Johnson-Cook constitutive equation for the material deformation. Johnson-Cook model governs material plasticity. Table 6 shows Johnson-Cook constants of Inconel 718 and Nimonic 80A. Johnson-Cook relation between strain rate and the temperature is as follows [16]:

$$\sigma = [A + B(\varepsilon_e^p)^n] \left[1 + Cln\frac{\dot{\varepsilon}}{\dot{\varepsilon}_0}\right] \left[1 - \left(\frac{T - T_r}{T_m - T_r}\right)^m\right] \tag{1}$$

Where T = temperature, Tm = melting point, ε_e^p and $\dot{\varepsilon}$ are effective plastic strain rate respectively, and A, B, C, n, m are material constants.

3 Governing Equations for Heat Transfer Model

Heat generation due to friction at the interface between the rotating tool and workpieces causes friction stir welding. In a static coordinate system, the Fourier law of heat conduction explains the heat transfer equation for tools in solid models. Temperature variation during friction stir welding is explained

by the equation as follows [19]:

$$\rho C_p \frac{\partial T}{\partial t} = \frac{\partial}{\partial x}\left(k_x \frac{\partial T}{\partial x}\right) + \frac{\partial}{\partial y}\left(k_y \frac{\partial T}{\partial y}\right) + \frac{\partial}{\partial}\left(\partial \frac{\partial T}{\partial Z}\right) \tag{2}$$

Where Cp: heat capacity, ρ: density, and k: heat conductivity. Newton's law of cooling is used to represent convection at the sides of the workpiece and tool.

$$k\frac{\partial T}{\partial n} = h\left(T - T_{amb}\right) \tag{3}$$

The torque required for rotation of tool is given by

$$\int_0^{M_R} dM = \int_0^R \mu P(r) 2\Pi r^2 dr = \frac{2}{3}\mu \Pi P r^3 \tag{4}$$

Where μ is the friction-coefficient, M is the interfacial torque, R is the surface radius, and $P(r)$ is the pressure distribution across the interface. Average heat input per unit area is given by

$$Q_1 = \int_0^R \omega \mu P(r) 2\Pi r^2 dr, \quad \text{Where } \omega = 2\Pi N, \tag{5}$$

Where ω is the angular velocity (rad/s), Q_1 is the net power (W) and P is the pressure [MPa]. Tool shoulder radius and rotation speed are identified as the main parameters by B Kiral in his studies on friction stir welding of an aluminium joint [20]. In this study, the frictional-coefficient was set to 0.3.

4 Description of Finite Element Model

Coupled Eulerian-Lagrangian formulation in Abaqus/Explicit software was used to simulate friction stir dissimilar welding of Inconel 718 and Nimonic 80A. During FSW, workpiece materials become viscous, which can be explained in a better manner using Eulerian analysis. From literature, plastic deformation and friction effect were the reasons for heat generation during FSW. The volume of the fluid method was used to implement the Eulerian method in Abaqus software. Material properties assigned to the finite element analysis for the present simulation studies are shown in Table 4.

The volume of the fluid method in Abaqus/explicit was used for Eulerian implementation. FSW tool is assigned with rigid body constraint and surface to surface contact is maintained between the FSW tool and workpiece surface. Tangential behavior, normal behavior, and heat generation properties are

Table 4 Physical and thermal properties of base and tool materials

	Density (g/cm^3)	Young's Modulus (GPa)	Thermal Conductivity (W/m.°C)	Specific Heat (J/g.°C)	Poisson's Ratio
Inconel 718	8.2	207	11.4	0.435	0.3
Nimonic 80A	8.19	222	11.2	0.448	0.3
WC-Co (Tool material)	3.9	600	70	0.350	0.3

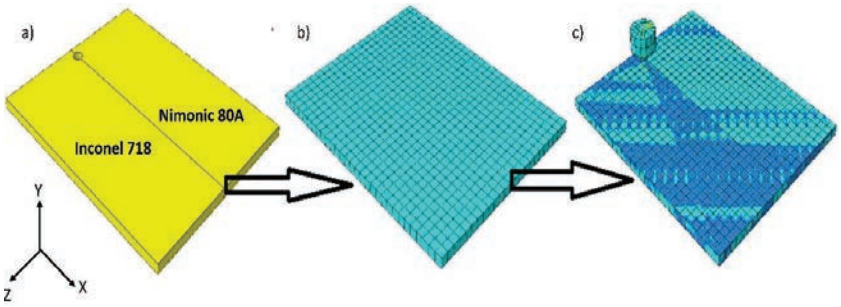

Figure 4 Coupled Eulerian-Lagrangian formulation: (a) Lagrangian body, (b) Eulerian body, (c) Coupled Eulerian-Lagrangian.

assigned as internal property to maintain the frictional property. A frictional coefficient of 0.3 was assigned. The energy caused by friction was fully converted to heat and fifty percentage of heat was transferred to the slave (workpiece) surface. Both Inconel 718 and Nimonic 80A were maintained at an initial temperature of 25°C. The bottom and side surfaces of both the workpieces were grounded by selecting Symmetry/Antisymmetry/Encastre type boundary condition and all movements were arrested. Three steps were assigned for this simulation study. Both displacement and rotatory movements were arrested for the initial step. Later for step 1, displacement of 4.8 mm along the negative y-axis was maintained as a part of FSW plunging with a force of 39.2 kN. Insertion depth should be such that the tool shoulder should come in proper contact with the workpiece to avoid defects like surface groove and inner channel. The tool was also provided with an rpm and the same rotation speed was maintained till the end of the process. Step 3 was assigned with a displacement along the x-axis to maintain welding travel speed and rotation about the y-axis. EC3D8RT, an 8-noded thermally coupled linear eulerian brick element type was used in this analysis for meshing. For Eulerian-lagrangian type simulation, the Lagrangian body need not have meshed. Eulerian-Lagrangian model is described in Figure 4.

After applying all the necessary conditions, the simulation was run for data check and was submitted for final analysis. From the results, the dependence of both tool rotation speed and travel speed on temperature variation was noted and graphs were plotted. From the results, a suitable tool rotation speed and travel speed were selected for further simulation studies such as tensile test and bend test.

5 Results and Discussion

In the present analysis, the heat generated due to friction between tool-shoulder and workpiece surfaces was considered. Whereas heat generated due to plastic deformation was not considered. The heat generated during FSW was one of the primary reasons for dynamic recrystallization that caused grain refinement. The dynamic recrystallization was known to occur at a temperature of 700°C. Improvement in mechanical properties of FSW joints was attributed to grain refinement. H Das in his paper on friction stir welding of Inconel 825 found that the mechanical performance of welded joint was significantly increased due to dynamic recrystallization and nanoprecipitation

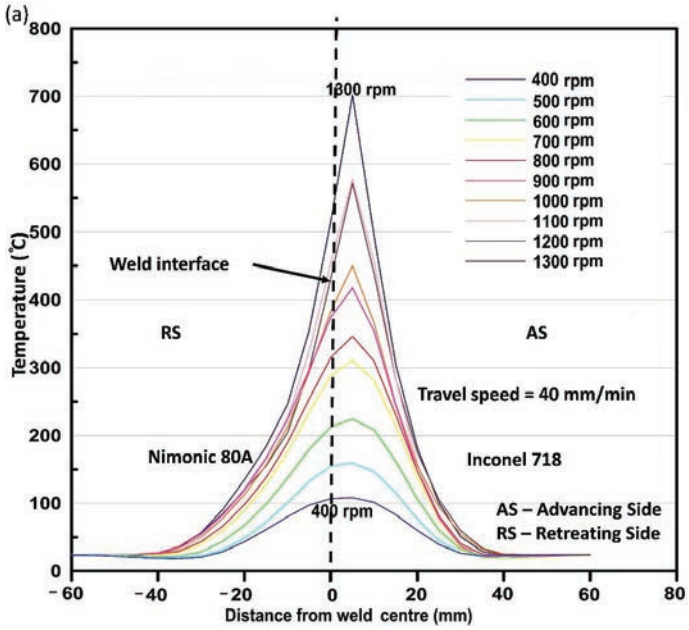

Figure 5 Temperature variation for trial R1.

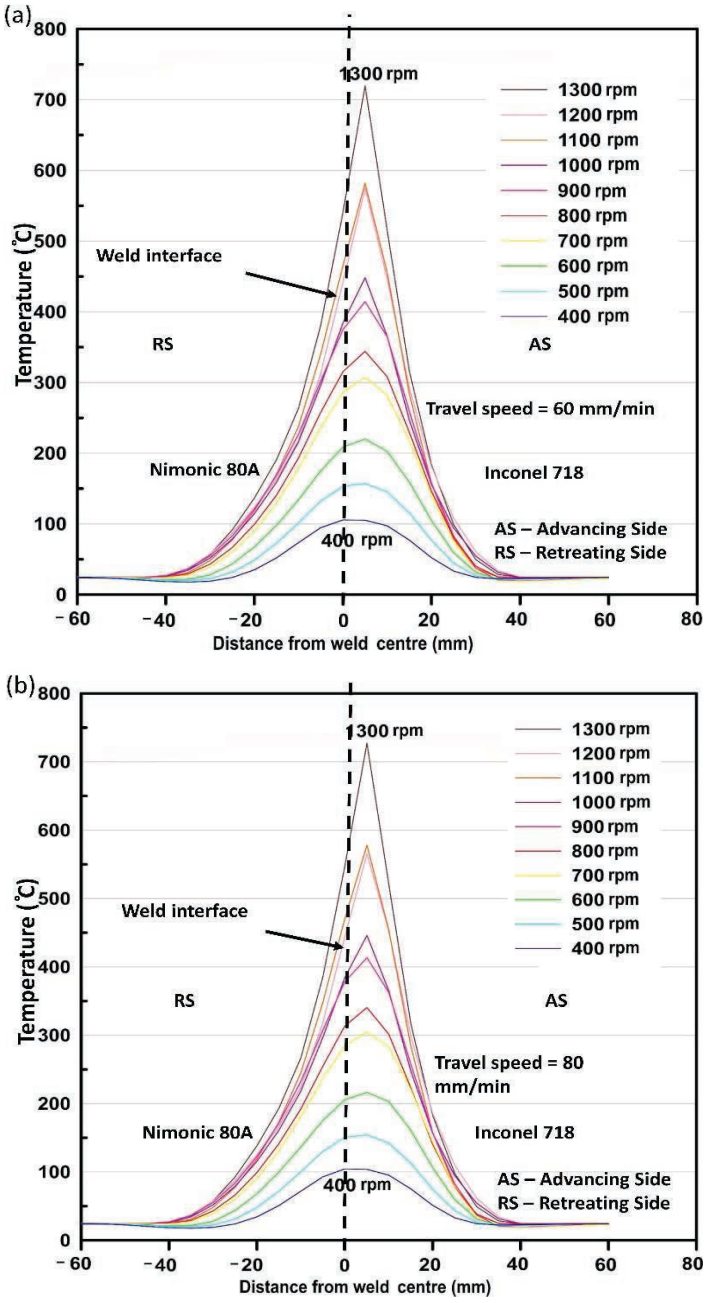

Figure 6 Temperature variation for (a) trial R2, (b) trial R3.

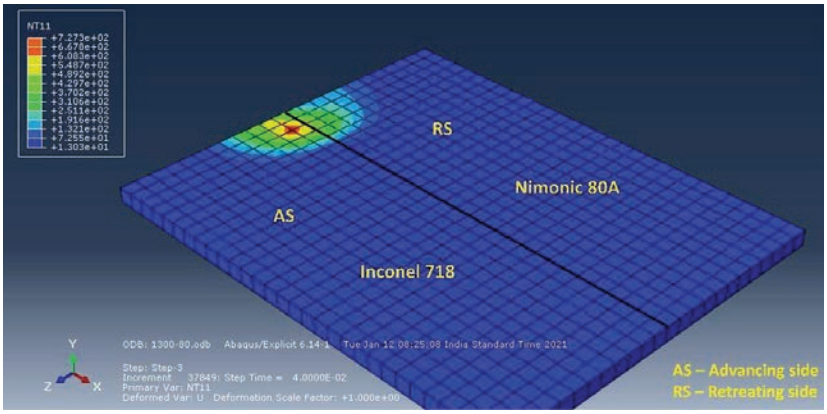

Figure 7 Temperature distribution for trial R3 using Abaqus software.

[21]. Rate of cooling after FSW was maintained to an optimum level to avoid grain growth. The high temperature in the stir zone can increase the dissolution of precipitates into the base matrix. Complete dissolution of precipitates can improve the properties and produce a strong weld.

From theoretical relation, there is a proportional relationship between rotation speed and heat generation, which is evident from Equation (5). Using Abaqus software, temperature distribution was obtained for all the trials. The temperature towards the advancing side was slightly higher than the retreating side. Peak-temperature was noticed at 3-4mm away from the weld interface. From the simulation results, an increase in temperature was noticed with an increase in tool rotation speed. Figure 5 shows a graph for a travel speed of 40mm/min. For a tool rotation speed of 1300 rpm at a travel speed of 40 mm/min, a peak nodal temperature of 701.57°C was noted. J Kangazian observed similar kind of results in his studies on friction stir dissimilar welding of Inconel 825 and 2507 super duplex stainless steel. Raising tool rotation speed increases heat input of FSW process and hence temperature rise [22]. Intense stirring and mixing of material due to an increase in tool rotation speed can also be a reason for higher temperature in the weld zone.

Nickel-based super-alloys like Inconel 718 have a low stack fault energy, compared to other materials like Al alloys that make these materials undergo easy dynamic recrystallization. Figure 6 shows the temperature distribution of R2 and R3 trials. Similar to the R1 trial, temperature increases with an

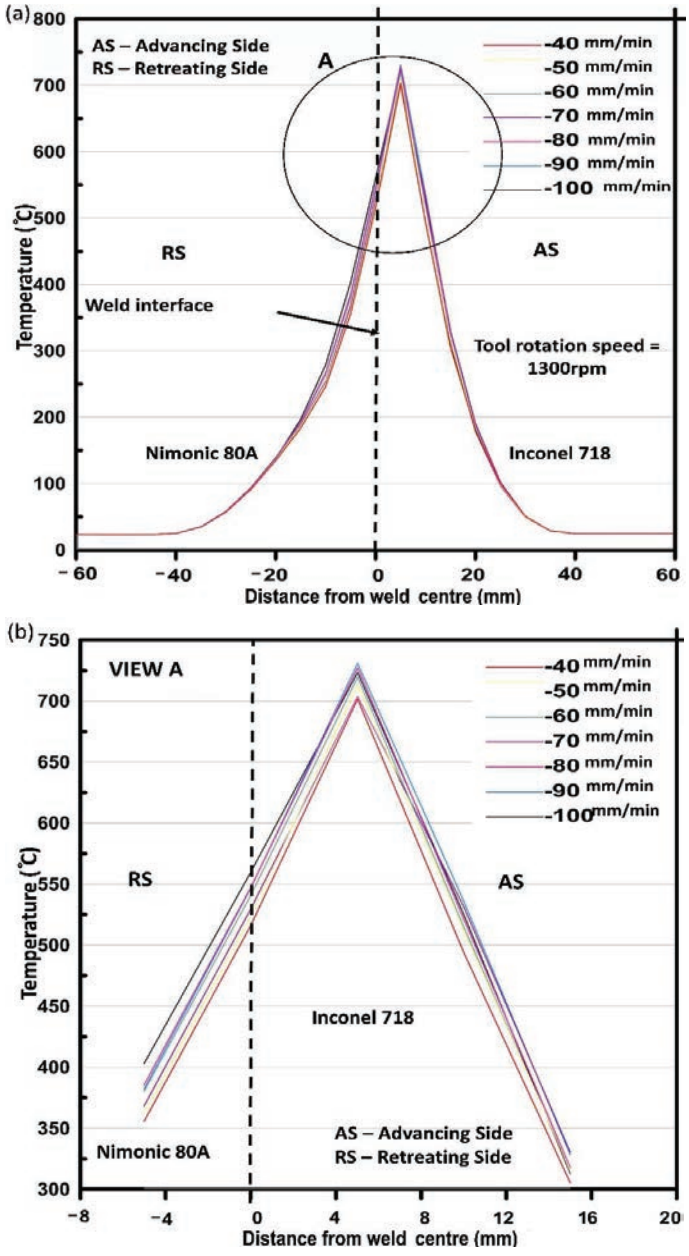

Figure 8 Temperature variation for (a) trial R4, (b) View A (refer to above figure).

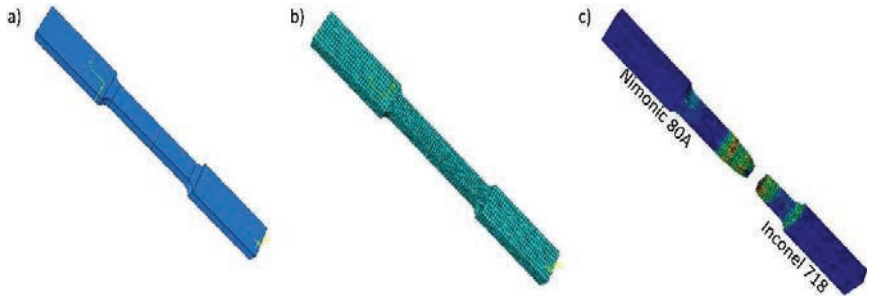

Figure 9 Tensile test specimen (a) unmeshed, (b) meshed (c) after the test (by simulation).

increase in tool rotation speed for both R2 and R3 trails. Peak temperature for R1, R2, and R3 trails was more than 700°C at a rotation speed of 1300 rpm.

Now, to understand the influence of travel speed on temperature distribution during FSW, travel speed is varied keeping tool rotation speed constant. For the R4 trail, travel speed is varied from 40 mm/min to 100 mm/min at a tool rotational speed of 1300 rpm. From the result, temperature distribution did not have a huge variation while changing the travel speed. From a closer look at the temperature plot from the R4 trail, with an increase in travel speed, there is a proportional increase in temperature distribution. Figure 8 explains the temperature plot for the R4 trail. An increase in travel speed can influence the stir zone grain size. K Song in his paper on friction stir welding of Inconel 600 mentioned that increase in travel speed results in refined grain size which causes improvement in mechanical properties [23]. M Ahmed observed a similar result in his investigation of friction stir weld Inconel 718 alloy. Hardness values of weld zone found a proportional relation with weld travel speed due to grain refinement in higher travel speed [24].

Tensile test for friction stir welded joint was carried out using Abaqus software. An improvement in mechanical properties was noticed in the friction stir weld specimen compared to the parent material. The tensile test specimen, meshed specimen, and final tensile tested result are shown in Figure 9. The tensile fracture occurred in the Inconel 718 base metal and the weld-zone was intact. M Ahmed In his paper on friction stir welding of Inconel 718 noticed an improvement in microhardness and strength for friction stir welded joint when compared to base material [25]. Grain refinement was one of the reasons for the improvement in weld specimen properties. From the stress-strain curve obtained from simulation, an increase in ultimate tensile strength was noticed. Ultimate tensile strength (UTS)

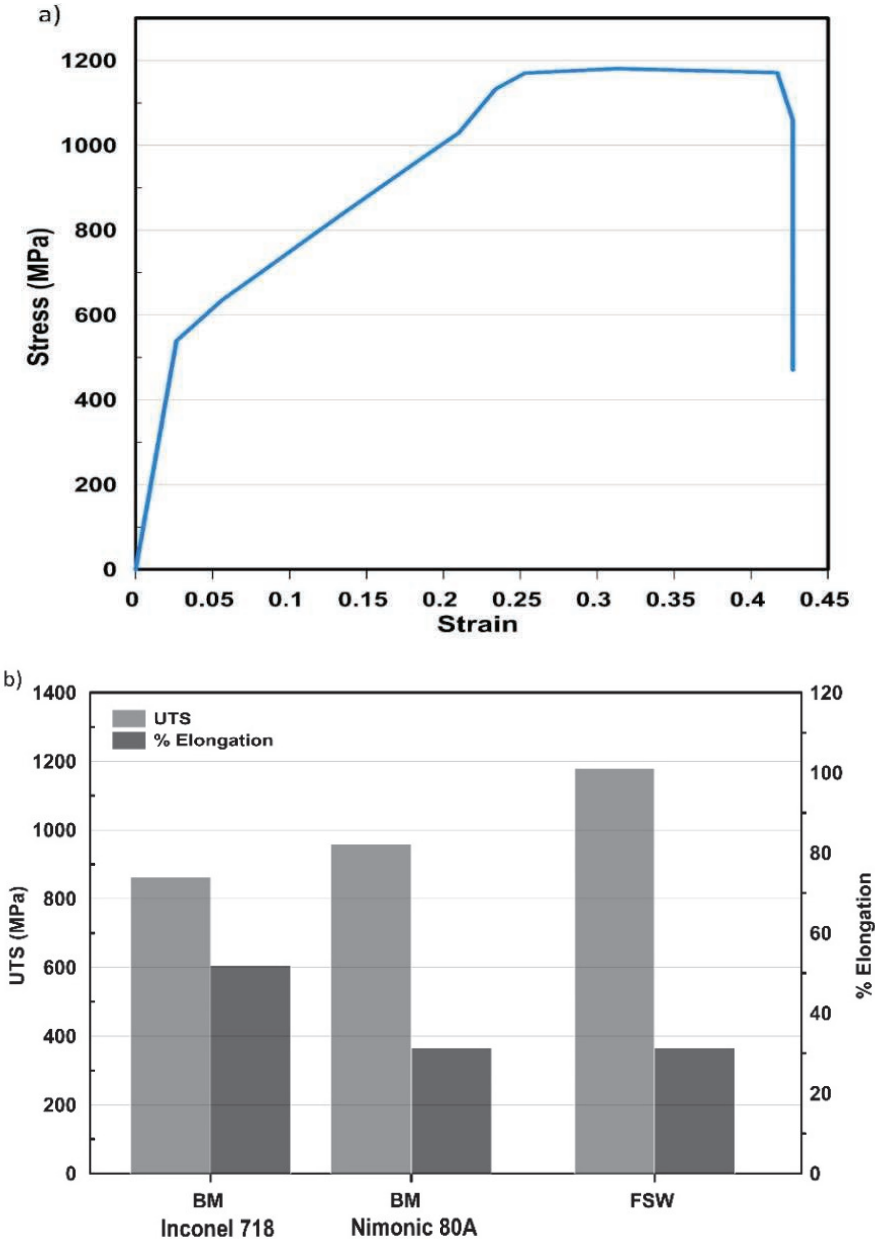

Figure 10 Transverse tensile test results: (a) Stress vs strain plot, (b) UTS and % Elongation of base material and FSW specimen.

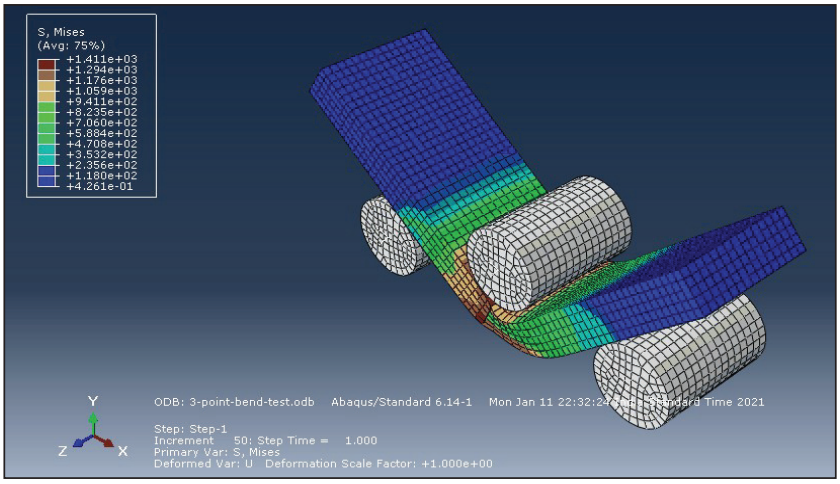

Figure 11 Bend test image after simulation.

and percent-elongation of Inconel 718 base metal were 886 MPa and 60% respectively [26]. From simulation results, UTS of FSW joint has increased to 1200 MPa, while elongation reduced to 31.3%. Hence there was an increase in tensile strength of almost 25% more than base material. This clearly explains the influence of grain refinement on mechanical properties. Similar to the above result, K Song noticed a 20% increase of ultimate tensile strength in friction stir welded Inconel 625 sample [27]. The stress-strain curve of the FSW weldment is shown in Figure 10(a). Comparison of UTS and percent-elongation for Inconel 718, Nimonic 80A, and FSW weldment is shown in Figure 10(b).

Using Abaqus tools, a three-point bend test was conducted and results were plotted. The bend-test specimen was designed as per ASTM-E290. The length and thickness of the specimen were 67.5 mm and 5 mm respectively. Weld-zone was at the center of the specimen. Distance between supports during bend-test was 37.5 mm. Simulation results for a deflection of 10 mm are noted. The bending stress-strain curve and Force – displacement curve were plotted from results. For a deflection of 6 mm, friction stir dissimilar weld was able to withstand a maximum load of 13958 N. A maximum stress of 1144 MPa at a strain of 0.36 was noted from the bend test. Bend test results in Abaqus software were given in Figure 11. Stress-strain curve and force vs displacement plot from bend test are shown in Figure 12.

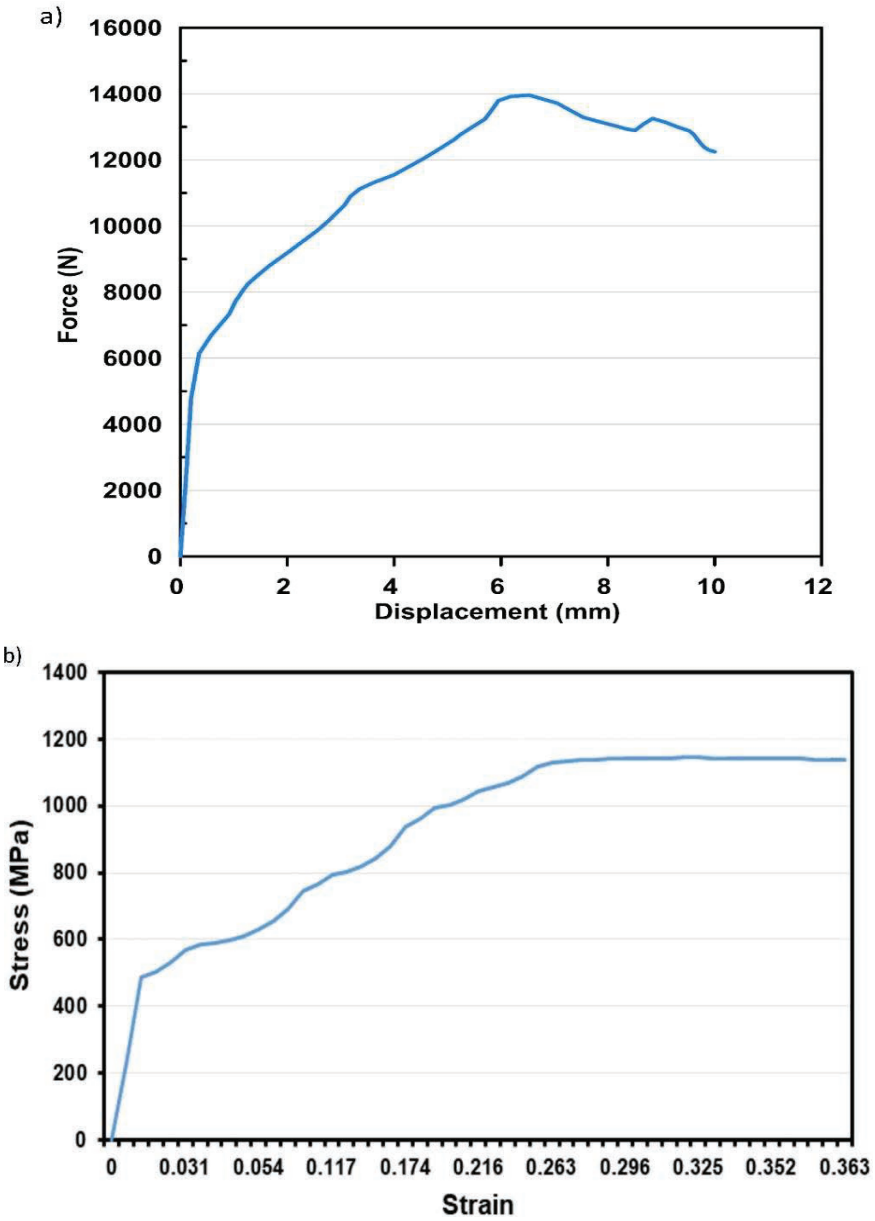

Figure 12 Bend test results after simulation: (a) Stress vs strain plot, (b) force vs displacement plot.

6 Conclusions

Heat generation during friction stir welding is caused by plastic deformation and friction. The effect of tool speed and travel speed on the temperature distribution in the weld zone was found by simulation of the FSW process using commercially available Abaqus software. Tensile and bend tests were also simulated. Mechanical properties better than the base metals were observed for the FSW weldments. The following conclusions can be drawn from the analysis.

- The temperature in the weld zone was found to increase with the increase in rotational speed when travel speed was held constant. This can be attributed to intense stirring and mixing of materials. The advancing side of the tool experienced higher temperatures than the retreating side.
- Temperature distribution remained nearly constant for different travel speeds when tool rotation speed was held constant.
- Simulated tensile test on transverse tensile specimens revealed a 25% increase in ultimate tensile strength and 50% reduction in percentage-elongation of FSW weldment in comparison to base metals.
- Simulated bend test on FSW weldment revealed a maximum load of 13958 N for a deflection of 6mm. Maximum bending stress of 1144 MPa at the maximum strain of 0.36 was also noticed.

References

[1] R. P. Singh, S. Dubey, A. Singh, and S. Kumar, "Materials Today: Proceedings A review paper on friction stir welding process," Mater. Today Proc., pp. 5–10, 2020.

[2] D. Deloison, C. Darcourt, A. Abisror, C. Decker, B. Journet, "Recent Advances in Welding Simulation of Aeronautical Components", Eur. J. Comput. Mech. (n.d.) 377–389.

[3] C. Sorensen and T. Nelson, "Friction stir welding of ferrous and nickel alloys," Frict. Stir Weld. Process., no. Ref 2, pp. 111–121, 2007.

[4] R. S. Mishra and Z. Y. Ma, "Friction stir welding and processing," Mater. Sci. Eng. R Reports, vol. 50, no. 1–2, pp. 1–78, 2005.

[5] D. Mishra, R. Basu, S. Dutta, S. K. Pal, and D. Chakravarty, "A review on sensor-based monitoring and control of friction stir welding process and a roadmap to Industry 4.0," J. Manuf. Process., vol. 36, no. November, pp. 373–397, 2018.

[6] R. Anand and V. G. Sridhar, "Studies on process parameters and tool geometry selecting aspects of friction stir welding – A review," Mater. Today Proc., vol. 27, pp. 576–583, 2020.
[7] A. A. O. Mmc, R. A. Prado, L. E. Murr, K. F. Soto, and J. C. Mcclure, "Self-optimization in tool wear for friction-stir welding of," vol. 349, pp. 156–165, 2003.
[8] S. Hirasawa, H. Badarinarayan, K. Okamoto, T. Tomimura, and T. Kawanami, "Analysis of effect of tool geometry on plastic flow during friction stir spot welding using particle method," J. Mater. Process. Technol., vol. 210, no. 11, pp. 1455–1463, 2010.
[9] Y. Tozaki, Y. Uematsu, and K. Tokaji, "Effect of tool geometry on microstructure and static strength in friction stir spot welded aluminium alloys," Int. J. Mach. Tools Manuf., vol. 47, no. 15, pp. 2230–2236, 2007.
[10] K. Gangwar and M. Ramulu, "Friction stir welding of titanium alloys: A review," Mater. Des., vol. 141, pp. 230–255, 2018.
[11] P. Gilles, D. Pont, E. Keim, J. Devaux, T. Areva, P. De, F.-P. Défense, R.J. Récamier, F.-L. Cedex, "Framatome-ANP Experience in Numerical Simulation o f Welding", Eur. J. Comput. Mech., 343–375, 2004.
[12] Thomas Dupuy, Chainarong Srikunwong, "Resistance Welding Numerical Simulation-A Promising Technique", Eur. J. Comput. Mech., 313–341, 2004.
[13] R. Fortunier, J.M. Bergheau, "Modelling of heat transfers, phase changes, and mechanical behaviour during welding", Eur. J. Comput. Mech., 231–245. 2004 https://doi.org/10.3166/reef.13.231-245.
[14] Special Metals, "IN718 Datasheet," pp. 1–28, 2007.
[15] Special Metals Corporation, "NIMONIC alloy 80A-Specification sheet," Smc-099, pp. 1–24, 2004.
[16] K. N. Salloomi, "Fully coupled thermomechanical simulation of friction stir welding of aluminium 6061-T6 alloy T-joint," J. Manuf. Process., vol. 45, no. June, pp. 746–754, 2019.
[17] H. K. Farahani, M. Ketabchi, and S. Zangeneh, "Determination of Johnson-Cook Plasticity Model Parameters for Inconel718," J. Mater. Eng. Perform., vol. 26, no. 11, pp. 5284–5293, 2017.
[18] M. E. Korkmaz and M. Günay, "Confirmation of Johnson-Cook Model Parameters for Nimonic 80A alloy by Finite Element Method," J. Polytech., vol. 0900, no. 3, pp. 625–632, 2019.

[19] V. Soundararajan, S. Zekovic, and R. Kovacevic, "Thermo-mechanical model with adaptive boundary conditions for friction stir welding of Al 6061," Int. J. Mach. Tools Manuf., vol. 45, no. 14, pp. 1577–1587, 2005.
[20] B. G. Kiral, M. Tabanoglu, and H. T. Serindag, "Finite element modeling of friction stir welding in aluminium alloys joint," Math. Comput. Appl., vol. 18, no. 2, pp. 122–131, 2013.
[21] H. Das, M. Mondal, S. T. Hong, J. W. Lee, and H. H. Cho, "Texture and precipitation behavior of friction stir welded Inconel 825 alloy," Mater. Today Commun., vol. 25, no. May, p. 101295, 2020.
[22] J. Kangazian and M. Shamanian, "Microstructure and mechanical characterization of Incoloy 825 Ni-based alloy welded to 2507 super duplex stainless steel through dissimilar friction stir welding," Trans. Nonferrous Met. Soc. China (English Ed., vol. 29, no. 8, pp. 1677–1688, 2019.
[23] K. H. Song, H. Fujii, and K. Nakata, "Effect of welding speed on microstructural and mechanical properties of friction stir welded Inconel 600," Mater. Des., vol. 30, no. 10, pp. 3972–3978, 2009.
[24] M. M. Z. Ahmed, B. P. Wynne, and J. P. Martin, "Effect of friction stir welding speed on mechanical properties and microstructure of nickel-based Super-alloy Inconel 718," Sci. Technol. Weld. Join., vol. 18, no. 8, pp. 680–687, 2013.
[25] M. M. Z. Ahmed, B. P. Wynne, and J. P. Martin, "Effect of friction stir welding speed on mechanical properties and microstructure of nickel-based Super-alloy Inconel 718," Sci. Technol. Weld. Join., vol. 18, no. 8, pp. 680–687, Nov. 2013.
[26] K. H. Song and K. Nakata, "Microstructural and mechanical properties of friction-stir-welded and post-heat-treated Inconel 718 alloy," J. Alloys Compd., vol. 505, no. 1, pp. 144–150, 2010.
[27] K. H. Song and K. Nakata, "Mechanical properties of friction-stir-welded Inconel 625 alloy," Mater. Trans., vol. 50, no. 10, pp. 2498–2501, 2009.

Biographies

Tom Saju is presently doing his Ph.D. in welding technology from the Vellore Institute of Technology. Vellore, Tamil Nadu, India. He has completed his M Tech in 2019 from Karunya Institute of Technology and Science, Coimbatore, Tamil Nadu, India, and B Tech degree in 2016 from Mahatma Gandhi University, Kerala, India. His area of interest includes similar and dissimilar welding technology, Finite element analysis, material characterization, fracture studies, etc.

M. Velu is an Associate Professor in the School of Mechanical Engineering, VIT University, Vellore, India. He received his Ph.D. in the field of Fracture and Fatigue of Dissimilar Welded Joints in 2015 from VIT University, Vellore, Tamil Nadu, India, M. E degree in Engineering Design from College of Engineering Guindy, Anna University, Chennai, Tamil Nadu, India in the year 1999 and B.E degree in Mechanical Engineering from University of Madras,

India in the year 1995. His area of interest includes Similar Welding, Dissimilar Welding, Fracture, and Fatigue of metals. He has more than 20 years of teaching experience and 10 years of research experience. He has published research papers in the field of Fracture, Fatigue, and Welding. Currently, he is working in the field of Fracture, Fatigue of Dissimilar Welded Joints of Ni-based Super-alloys for Gas Turbine applications.